Fourier Transform Ultraviolet Spectroscopy of the A $^2\Pi_{3/2} \leftarrow$ X $^2\Pi_{3/2}$ Transition of BrO†

David M. Wilmouth,* Thomas F. Hanisco, Neil M. Donahue, and James G. Anderson

Department of Chemistry and Chemical Biology, Harvard University, Cambridge, Massachusetts 02138

Received: May 19, 1999; In Final Form: August 23, 1999

The first spectra of the A $^2\Pi_{3/2} \leftarrow$ X $^2\Pi_{3/2}$ electronic transition of BrO using Fourier transform ultraviolet spectroscopy are obtained. Broadband vibrational spectra acquired at 298 ± 2 K and 228 ± 5 K, as well as high-resolution rotational spectra of the A ← X 7,0 and 12,0 vibrational bands are presented. Wavenumber positions for the spectra are obtained with high accuracy, and cross section assignments are made, incorporating the existing literature. With 35 cm^{-1} (0.40 nm) resolution the absolute cross section at the peak of the 7,0 band is determined to be $(1.58 \pm 0.12) \times 10^{-17}$ cm^2 $molecule^{-1}$ at 298 ± 2 K and $(1.97 \pm 0.15) \times 10^{-17}$ cm^2 $molecule^{-1}$ at 228 ± 5 K. BrO dissociation energies are determined with a graphical Birge−Sponer technique, using Le Roy−Bernstein theory to place an upper limit on the extrapolation. From the ground-state dissociation energy, $D_0'' = 231.0 \pm 1.7$ kJ/mol, the heat of formation of BrO(g) is calculated, $\Delta_f H°(0\ K) = 133.7 \pm 1.7$ kJ/mol and $\Delta_f H°(298.15\ K) = 126.2 \pm 1.7$ kJ/mol. Cross sections for the high-resolution 7,0 and 12,0 rotational peaks are the first to be reported. The band structures are modeled, and improved band origins, rotational constants, centrifugal distortion constants, and linewidths are determined. In particular, *J*-dependent linewidths and lifetimes are observed for the both the 7,0 and 12,0 bands.

Introduction

It is now well-established that bromine compounds, which enter the atmosphere from a variety of natural and anthropogenic sources, cause stratospheric and tropospheric ozone depletion.[1−9] Despite being present at much lower atmospheric concentrations than chlorine compounds, bromine compounds are much more efficient at ozone destruction on a per atom basis. This is because a large fraction of inorganic bromine is present in chemically active forms, while most inorganic chlorine is sequestered in the relatively long-lived reservoirs, HCl and $ClONO_2$. Only a few percent of the total inorganic chlorine in the stratosphere is in the reactive form ClO, while more than half of the inorganic bromine is present as reactive BrO during daylight. At altitudes below 25 km the BrO/ClO and BrO/HO_2 cycles are among the most important ozone destruction cycles.[5,7]

Current knowledge of BrO in the atmosphere has been aided by a number of remote sensing measurements,[6,10−20] which utilized the BrO near-ultraviolet (UV) absorption spectrum. The spectrum has well-defined vibrational band structure and is assigned to the A $^2\Pi_{3/2} \leftarrow$ X $^2\Pi_{3/2}$ electronic transition.[21,22] Most of the bands are completely diffuse owing to rapid predissociation, although a few exhibit rotational structure at high resolution.[21−23] The spectral features of the vibrational bands provide the characteristic signature that has been used to detect BrO in numerous atmospheric[6,10−20] and laboratory measurements.[24−27]

The earliest spectra of the A ← X bands in BrO were observed in the emission of flames.[28,29] Durie and Ramsay[22] first detected the UV absorption of BrO, following the flash photolysis of Br_2-O_2 mixtures. They presented vibrational and rotational analyses and determined dissociation energies. Loewenschuss et al.[30] observed the absorption spectrum of BrO from argon matrix samples and revised the gas-phase vibronic assignments of Durie and Ramsay.[22] Barnett et al.[21] obtained absorption spectra of normal BrO and isotopically enriched ^{81}BrO using flash photolysis of mixtures of bromine and ozonized oxygen. They presented vibrational and rotational analyses and described a number of previously unseen hotbands. The first study to assign cross sections as a function of wavelength to the BrO spectrum was conducted by Cox et al.[24] Subsequently, Wahner et al.[31] determined the absolute UV cross sections for BrO in the wavelength range 312−385 nm at 298 and 223 K. The Wahner et al.[31] spectra have been used as the BrO reference spectra in numerous atmospheric studies over the past decade and are presented in the NASA JPL-97 compendium.[32] Additional measurements of the BrO cross sections have been reported by Orlando et al.[33] and Gilles et al.[26] over a broad wavelength range, and by Laszlo et al.[34] at the 7,0 peak. Recently, cavity ring-down rotational spectra of the 7,0 and 12,0 bands were analyzed by Wheeler et al.[23]

Reference spectra with accurate wavelengths are extremely important for atmospheric measurements,[18,35] particularly for deconvolving overlapping spectral features of different molecules. UV cross sections of BrO are needed to interpret laboratory and field measurements and to estimate the photolytic destruction of BrO in atmospheric models.[31] With the onset of the Global Ozone Monitoring Experiment (GOME), there is now the first possibility of establishing a global climatology of BrO, and the need for new, accurate BrO reference spectra is substantial.[18]

The heat of formation is essential for understanding the thermodynamics of important atmospheric and combustion reactions involving BrO. There is presently significant uncertainty in the literature regarding this value.[36−38] The need for accurate measurements of the dissociation energy and heat of formation of BrO has recently been addressed.[39] Similarly, there have been two previous studies[21,23] that determined spectro-

* Corresponding author. E-mail: wilmouth@huarp.harvard.edu. Fax: 617-495-4902.

† Spectra obtained in this study are available from the authors upon request.

10.1021/jp991651o CCC: $18.00
Published on Web 10/27/1999

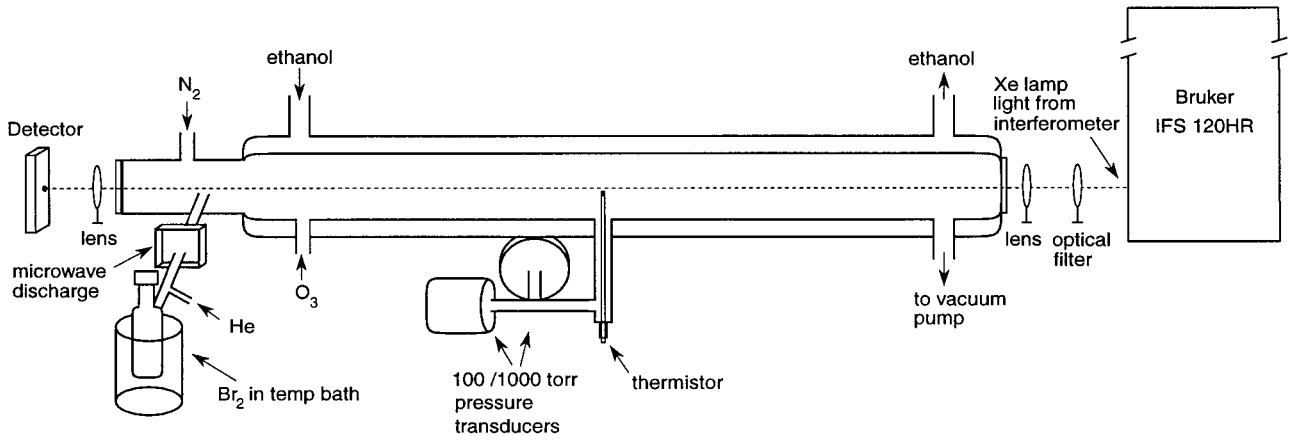

Figure 1. Experimental apparatus.

scopic constants from the rotational structure of the BrO 7,0 and 12,0 vibrational bands, but additional work is needed to improve these values.

In this study, we obtain ambient and low-temperature BrO vibrational spectra of high wavenumber accuracy using the Fourier transform technique and assign cross sections based on an analysis of existing cross section data. From a graphical extrapolation of the vibrational energy intervals we determine the dissociation energy and thereby the heat of formation of BrO(g). We also present high-resolution rotational spectra of the 7,0 and 12,0 bands, providing cross sections for the rotational peaks and determining spectroscopic constants.

Experiment

Spectra were acquired in this study using a high-resolution Fourier transform spectrometer (Bruker IFS 120HR). The spectrometer has previously been used in this laboratory to study the 2-0 band of the A ← X transition in IO.[40] The Fourier Transform technique offers a number of well-known advantages over dispersive spectroscopy, in particular, higher wavenumber accuracy (Connes advantage). High wavenumber precision is achieved by referencing the sample interferogram to the zero crossings of the interferogram from a frequency-stabilized helium−neon laser. Absolute wavenumber errors can still occur, however, so calibration is necessary to ensure accuracy. The sharp absorption features of iodine in the range 17 600−18 300 cm^{-1} were used for the absolute wavenumber calibration in this study. Twenty relatively isolated, symmetric peaks of normal width and intensity were selected and referenced to the corrected iodine atlas of Gerstenkorn and Luc[41] in order to determine the small absolute correction factor to apply to our BrO spectra.

The experimental apparatus is shown in Figure 1. BrO was produced in a double-jacketed 1-m glass fast flow reactor via the reaction

$$Br + O_3 \rightarrow BrO + O_2 \qquad (1)$$

Bromine atoms were formed by extracting the vapor over liquid Br_2 and passing it through a microwave plasma with UHP helium carrier gas. Oxygen was passed through an electric discharge to produce approximately 7% O_3 in O_2. Typical experimental pressures were 25 Torr He, 5 Torr O_3/O_2, and 5 Torr N_2 carrier gas. Pressure transducers were used to continuously monitor the system pressure, and a thermistor at the center of the gas flow was used to monitor the temperature. Low temperatures were achieved by pumping chilled ethanol through the outer jacket of the flow tube. Thermistors placed at either end of the tube allowed the temperature gradient to be determined. Absorption was measured using a spectrally filtered 75 W xenon arc lamp source and a silicon photodiode detector.

The experimental procedure was to first obtain a background spectrum with all gases flowing, but with the microwave discharge off, and then to obtain a sample spectrum of BrO with the discharge on. The ratio of these raw spectra constituted a single transmittance measurement. A typical background-sample sequence included 50−200 scans. Thousands of scans were acquired and averaged to produce each of the spectra presented here. Bromine and ozone spectra were also obtained in order to subtract out their overlapping absorptions in the BrO spectra.

Data were acquired at two different temperatures: 298 and 228 K. On the basis of temperature fluctuations and gradient information, the uncertainty in the ambient-temperature measurements is ±2 K, and the uncertainty in the low-temperature measurements is ±5 K. The BrO vibrational spectra were acquired at 10 cm^{-1} resolution, while the 7,0 and 12,0 rotational spectra were acquired at 0.5 cm^{-1} resolution. All spectra were obtained with no apodization function, i.e., boxcar truncation.

The interferometer was maintained at atmospheric pressure during our measurements. Following acquisition, the spectral wavenumbers were corrected for the index of refraction of air and are reported here in vacuum. Conservative wavenumber uncertainties are ±0.2 cm^{-1} for the 10 cm^{-1} spectra and ±0.02 cm^{-1} for the 0.5 cm^{-1} spectra. Unless otherwise stated, all uncertainties are reported as $\pm 1\sigma$.

Results

A. Vibrational Data. *Spectra and Cross Sections.* The BrO vibrational spectra at 298 ± 2 K and 228 ± 5 K are shown in Figure 2. The vibrational transitions (v',v'') are listed at the top of the 298 ± 2 K spectrum. We observe the strongly structured v',0 progression from $v' = 0$ to $v' = 26$, extending the range of reported transitions. The 1,1; 2,1; and 4,1 hotbands are also seen at 298 ± 2 K, while only the 4,1 is seen at 228 ± 5 K.

Cross sections were not experimentally determined in this study due to uncertainties in concentrations over our long absorption path length. The absorption cross sections in Figure 2 were determined from an analysis of the existing literature. The apparent BrO cross sections are resolution dependent, so much of the literature data cannot be directly compared since most studies were performed at different resolutions. To circumvent this difficulty and to obtain the most accurate cross section information possible, the 10 cm^{-1} BrO absorption spectra

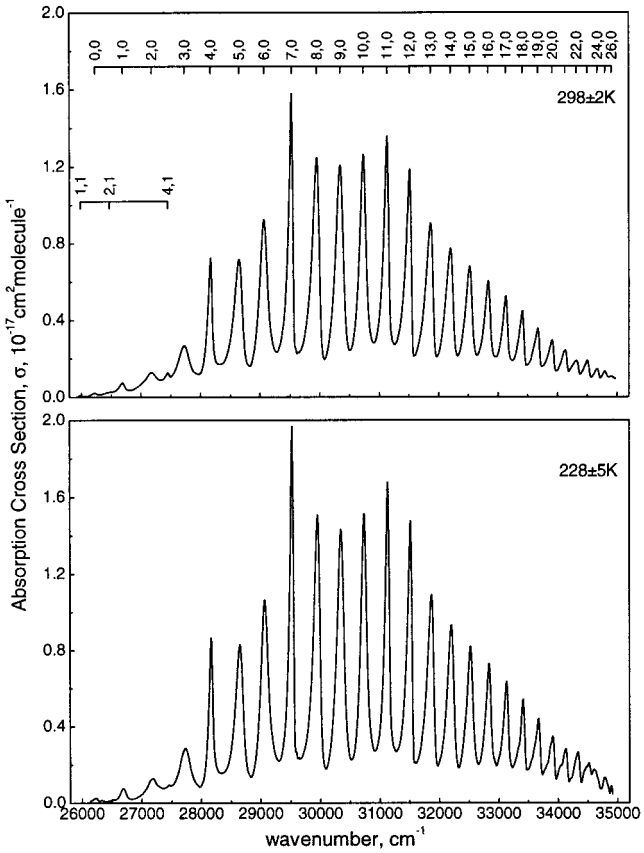

Figure 2. UV absorption spectra of the A $^2\Pi_{3/2} \leftarrow X\ ^2\Pi_{3/2}$ transition of BrO at 298 ± 2 K and 228 ± 5 K. Spectra were acquired at 10 cm^{-1} resolution with no apodization and are displayed here degraded to 35 cm^{-1} resolution with triangular apodization. Cross sections are normalized to the 7,0 band cross section. The vibrational transitions (v',v'') are listed at the top of the 298 K spectrum.

TABLE 1: BrO Absorption Cross Sections for the 7,0 Band at 298 K

ref	reported resolution (nm)	σ^a at reported resolution absolute	σ^a at reported resolution differential[b]	$\sigma^{a,c}$ at 0.40 nm resolution absolute	$\sigma^{a,c}$ at 0.40 nm resolution differential[b]
24	0.22	1.8	1.6	1.6	1.4
31	0.40	1.55	1.25	1.55	1.25
33	0.40	1.4	1.2	1.4	1.2
26	0.50	1.63	1.44	1.74	1.55
34	0.60	1.41		1.59	
average				1.58	1.35

[a] Cross section units are 10^{-17} cm^2 $molecule^{-1}$. [b] Differential cross sections are reported from the apex of the 7,0 band to the valley at the higher wavenumber side. [c] Cross sections at 0.40 nm were determined by degrading our 10 cm^{-1} (0.11 nm at the 7,0 peak) BrO absorption spectrum to the reported resolutions, determining the multiplicative factor and additive factor necessary to match the cross sections, and applying those factors to our spectrum when degraded to 0.40 nm at the 7,0 peak.

acquired in this study were used to analyze the existing literature at a common resolution. The results at 298 K are shown in Table 1.

Each reference in Table 1 is listed with its reported spectral resolution and absolute cross section for the 7,0 band. The 7,0 is the largest vibrational peak, and it is the one historically used in the determination of the BrO cross section. Only Gilles et al.[26] explicitly stated the differential cross section, determined from the apex of the 7,0 band to the valley at the higher wavenumber side. The differential cross section for Wahner et al.[31] was obtained from the spectrum in digital form, and for Cox et al.[24] and Orlando et al.,[33] it was obtained by analyzing the published figures. Laszlo et al.[34] reported no spectra, so the differential cross section could not be determined. The reference cross sections were converted to a resolution of 0.40 nm for comparison, using the following procedure. Our 298 K 10 cm^{-1} (0.11 nm at the 7,0 peak) BrO spectrum was degraded to the resolution of each study, with a triangular apodization function applied in order to match the dispersive spectroscopy instrument line function. Once degraded, the multiplicative factor and additive factor necessary to match the reference cross sections were determined. These factors were then applied to our spectrum degraded to 0.40 nm (35 cm^{-1}) resolution at the 7,0 peak. The resulting absolute and differential cross sections are listed in the right-hand columns of Table 1. Averaging these results yields a 7,0 band absolute cross section of 1.58×10^{-17} cm^2 $molecule^{-1}$ and a differential cross section of 1.35×10^{-17} cm^2 $molecule^{-1}$. Taking the standard deviation of the measurements as the uncertainty gives $\pm 0.12 \times 10^{-17}$ (±8%) for the absolute and $\pm 0.15 \times 10^{-17}$ (±11%) cm^2 $molecule^{-1}$ for the differential cross section.

Only two low-temperature cross section measurements at the 7,0 band have previously been performed. At 223 K and 0.40 nm resolution, Wahner et al.[31] found an absolute cross section of 1.95×10^{-17} cm^2 $molecule^{-1}$ and a differential cross section of 1.66×10^{-17} cm^2 $molecule^{-1}$. The 222 K, 0.50 nm resolution Gilles et al.[26] spectrum converted to 0.40 nm resolution corresponds to an absolute cross section of 2.21×10^{-17} cm^2 $molecule^{-1}$ and a differential cross section of 2.00×10^{-17} cm^2 $molecule^{-1}$. A simple average of these results has a relatively large uncertainty, so we instead determined the low-temperature cross sections using the observed linear temperature dependence[26] of the BrO cross sections. The ratios of the values at 228 and 298 K ($\sigma_{228K}/\sigma_{298K}$) were determined for each study and found to be essentially identical (1.245 ± 0.006 for the absolute and 1.287 ± 0.027 for the differential cross section). These ratios were applied to the average 298 K cross sections shown in Table 1 to yield a 228 K absolute cross section of $(1.97 \pm 0.15) \times 10^{-17}$ cm^2 $molecule^{-1}$ and a differential cross section of $(1.74 \pm 0.20) \times 10^{-17}$ cm^2 $molecule^{-1}$.

By normalizing to the 7,0 band absolute and differential cross sections, the cross sections for the other vibrational bands in Figure 2 were assigned. The spectra are shown degraded to 35 cm^{-1} resolution with triangular apodization in order to match the 7,0 band cross sections to the 0.40 nm resolution values determined from the literature analysis. The band positions and absolute cross sections from Figure 2 are summarized in Table 2. The wavenumbers correspond to the apex of each 298 ± 2 K spectrum band and are intended merely as a guide to the peak positions. The band position wavenumbers vary with resolution and temperature; at higher resolution and lower temperature the peak positions generally appear shifted to higher wavenumbers. The uncertainties in the absolute cross sections are listed in parentheses as a percentage of each respective cross section value. Bands in the middle of the spectra are assigned the same uncertainty as the reference 7,0 band. The greater uncertainty in the cross sections at the ends of the spectra results from the removal of the overlapping absorption of Br_2 at low wavenumbers and O_3 at high wavenumbers. Both molecules exhibit an unstructured absorption continuum, which appeared in the BrO spectra as a baseline shift. To correct for this, Br_2 and O_3 spectra were acquired and subtracted from the BrO spectra by an amount necessary to yield a zero cross section at the observed wavenumber extremes.

TABLE 2: BrO Band Positions and Absolute Absorption Cross Sections[a]

v',v''	cm^{-1} [b]	σ at 298 ± 2 K[c]	σ at 228 ± 5 K[c]
1,1	25982.9	9.86×10^{-20} (*d*)	*e*
0,0	26227.9	2.25×10^{-19} (*d*)	2.74×10^{-19} (*d*)
2,1	26470.8	2.75×10^{-19} (40)	*e*
1,0	26688.7	7.45×10^{-19} (14)	7.73×10^{-19} (16)
2,0	27178.6	1.28×10^{-18} (9)	1.29×10^{-18} (9)
4,1	27448.5	1.26×10^{-18} (9)	9.54×10^{-19} (9)
3,0	27728.2	2.67×10^{-18} (8)	2.87×10^{-18} (8)
4,0	28167.8	7.23×10^{-18} (8)	8.64×10^{-18} (8)
5,0	28646.1	7.15×10^{-18} (8)	8.28×10^{-18} (8)
6,0	29066.5	9.23×10^{-18} (8)	1.06×10^{-17} (8)
7,0	29525.4	1.58×10^{-17} (8)	1.97×10^{-17} (8)
8,0	29949.7	1.25×10^{-17} (8)	1.51×10^{-17} (8)
9,0	30343.1	1.21×10^{-17} (8)	1.43×10^{-17} (8)
10,0	30734.5	1.26×10^{-17} (8)	1.51×10^{-17} (8)
11,0	31133.7	1.36×10^{-17} (8)	1.67×10^{-17} (8)
12,0	31517.4	1.19×10^{-17} (8)	1.48×10^{-17} (8)
13,0	31866.5	9.04×10^{-18} (8)	1.09×10^{-17} (8)
14,0	32202.0	7.72×10^{-18} (8)	9.32×10^{-18} (8)
15,0	32524.1	6.79×10^{-18} (8)	8.19×10^{-18} (8)
16,0	32836.4	6.01×10^{-18} (8)	7.28×10^{-18} (8)
17,0	33133.4	5.23×10^{-18} (8)	6.36×10^{-18} (8)
18,0	33411.1	4.47×10^{-18} (8)	5.41×10^{-18} (8)
19,0	33673.4	3.56×10^{-18} (8)	4.41×10^{-18} (8)
20,0	33912.5	2.95×10^{-18} (9)	3.48×10^{-18} (10)
21,0	34130.4	2.42×10^{-18} (10)	2.84×10^{-18} (12)
22,0	34317.4	1.88×10^{-18} (13)	2.67×10^{-18} (14)
23,0	34502.6	1.88×10^{-18} (15)	2.08×10^{-18} (20)
24,0	34668.4	1.45×10^{-18} (21)	1.75×10^{-18} (25)
25,0	34797.6	1.32×10^{-18} (25)	1.33×10^{-18} (38)
26,0	34909.4	1.07×10^{-18} (34)	8.83×10^{-19} (*d*)

[a] Spectral resolution is 35 cm^{-1}, triangular apodization. [b] Wavenumbers (cm^{-1}) listed are for the apex of each band in the 298 K spectrum. [c] Cross section units are cm^2 $molecule^{-1}$. Numbers in parentheses are ±% uncertainties. [d] Uncertainty is greater than 50%; cross sections are listed only as a guide. [e] The 1,1 and 2,1 hotbands were not observed at 228 K.

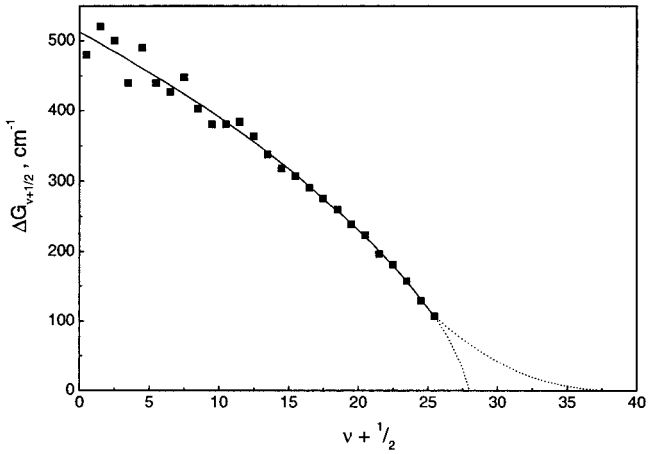

Figure 3. Birge−Sponer plot of the vibrational level intervals of the A state of BrO. The solid line is fit through the observed data points, while the dotted lines are the extrapolations representing the minimum and maximum dissociation energies.

Dissociation Energy and Heat of Formation. The BrO excited state dissociates into $Br(^2P_{3/2}) + O(^1D_2)$.[22] Using a graphical Birge−Sponer extrapolation, in which the vibrational energy separations, $\Delta G_{v+1/2}$, are plotted versus $v + {}^1/_2$, the dissociation energy can be found. The Birge−Sponer plot for BrO is shown in Figure 3. The solid line fit through our data points displays negative curvature, which increases at the highest observed values of v. Extrapolating the curve (not shown) yields a value for the unobserved dissociation limit, v_D, of 29 ± 1, and an A ← X dissociation energy of 35 090 ± 50 cm^{-1}. The scatter in the $\Delta G_{v+1/2}$ values at low vibrational numbers, caused by imprecise determination of the band origins from the 10 cm^{-1} spectrum, does not contribute significantly to the uncertainty since the dissociation energy was found by adding the extrapolated vibrational intervals to the last observed energy level. The dissociation energy was also derived from the area under the extrapolated curve and found to be in good agreement with this result. However, caution must be taken in applying this extrapolation. The upper states of a number of diatomics, including the halogens Cl_2,[42,43] Br_2,[43,44] and I_2,[43,45] and ClO[46] and O_2[47] exhibit a "tail", i.e., an inflection to positive curvature in Birge−Sponer plots at high v. This positive curvature is caused by long-range attractive interactions near the dissociation limit. It is likely that BrO also shows this behavior at vibrational levels beyond those observed here and that the dissociation limit from the Birge−Sponer extrapolation underestimates the true value.

Le Roy and Bernstein have developed a procedure that corrects for the positive curvature commonly observed in the tail of Birge−Sponer extrapolations by making use of the known form of the long-range interaction of two atoms.[43,48−50] A useful result of the Le Roy-Bernstein theory is that a plot of $(\Delta G_{v+1/2})^{(\tilde{n}-2)/(\tilde{n}+2)}$ versus $v + {}^1/_2$ shows negative curvature for deeper vibrational levels and is a straight line at long range. Hence, a linear extrapolation from such a plot should always provide an upper limit to the dissociation energy.[43] Here $\tilde{n}$ is the limiting value of the effective inverse power of the long-range potential, typically 5 or 6 for a neutral molecule. In the absence of any observed positive curvature in the Birge−Sponer plot for BrO, we place a conservative upper bound on the dissociation energy by considering $\tilde{n} = 5$ and extrapolating a line from the last five observed data points on a plot of $(\Delta G_{v+1/2})^{3/7}$ versus $v + {}^1/_2$. This yields a maximum value for the A ← X dissociation energy of 35 310 cm^{-1}. The positive curvature in the Birge−Sponer plot necessary to produce this upper limit is shown as a dotted line in Figure 3, along with a dotted line for the lower limit of 35 040 cm^{-1} determined from the lower limit of the Birge−Sponer extrapolation. With these upper and lower bounds we therefore report an A ← X dissociation energy of 35 180 ± 140 cm^{-1} and an excited-state dissociation energy, $D_0' = 8930 \pm 140$ cm^{-1} at the 2σ level. Subtracting the $^1D_2-{}^3P_2$ excitation energy of the oxygen atom (15 867.862 cm^{-1}) from 35 180 cm^{-1} yields a BrO ground-state dissociation energy, $D_0'' = 19\,312 \pm 140$ cm^{-1} or 231.0 ± 1.7 kJ/mol.

The ground-state dissociation energy was used to determine the heat of formation of BrO(g). $\Delta_f H°$ for BrO(g) is defined by

$$ {}^1/_2Br_2(l) + {}^1/_2O_2(g) \rightarrow BrO(g) \qquad (2) $$

Replacing the reaction by a hypothetical two-step process yields

$$ {}^1/_2Br_2(l) + {}^1/_2O_2(g) \rightarrow Br(g) + O(g) \qquad (3) $$

$$ Br(g) + O(g) \rightarrow BrO(g) \qquad (4) $$

where the sum of the hypothetical reactions is reaction 2, and $\Delta_f H° = \Delta H_3 + \Delta H_4$. The enthalpy of reaction 3 can be calculated, and the enthalpy of reaction 4 is the negative of the BrO ground-state dissociation energy. Using data from the NIST-JANAF Thermochemical Tables[36] and the dissociation energy determined here, we find $\Delta_f H°(0\ K) = 133.7 \pm 1.7$ kJ/mol and $\Delta_f H°(298.15\ K) = 126.2 \pm 1.7$ kJ/mol at the 2σ level.

B. Rotational Data. *7,0 Band.* The ambient temperature (298 ± 2 K) rotational spectrum of the BrO A $^2\Pi_{3/2}$ ← X $^2\Pi_{3/2}$ 7,0 band is shown in Figure 4. The spectrum was acquired at 0.5 cm^{-1} resolution and is shown here degraded to 1.0 cm^{-1}

TABLE 3: BrO A $^2\Pi_{3/2}$ State Molecular Constants in cm^{-1}

constant	^{79}BrO[a]	^{81}BrO[a]	±unc[b]	^{79}BrO[c]	^{81}BrO[c]	^{79}BrO[d]	^{81}BrO[d]
$\nu_{0\ 7,0}$	29547.18	29542.09	0.05	29547.3(8)	29542.5(8)	29543.59(110)	29538.59(71)
B_7	0.29334	0.29210	0.0002	0.292(2)	0.290(2)	0.28812(170)	0.28672(82)
D_7	8×10^{-7}	8×10^{-7}	3×10^{-7}			$[8.8 \times 10^{-7}]^e$	$[8.8 \times 10^{-7}]^e$
Γ_7	$2.10 + 4.6 \times 10^{-4}[J(J+1)] + 3.6 \times 10^{-6}[J(J+1)]^2$	$1.95 + 4.9 \times 10^{-4}[J(J+1)] + 2.8 \times 10^{-6}[J(J+1)]^2$	0.1	3.2(3)	3.2(3)		2.8
$\nu_{0_{12,0}}$	31547.45	31539.59	0.3	31545.7(8)	31538.5(9)	31547.74(55)	31539.88(22)
B_{12}	0.27279	0.27166	0.0005	0.273(3)	0.271(3)	0.27244(39)	0.27141(32)
D_{12}	10×10^{-7}	10×10^{-7}	3×10^{-7}			$[8.8 \times 10^{-7}]^e$	$8.8(11) \times 10^{-7}$
Γ_{12}	$7.42-8.0 \times 10^{-3}[J(J+1)] + 3.3 \times 10^{-6}[J(J+1)]^2$	$7.90-7.5 \times 10^{-3}[J(J+1)] + 2.7 \times 10^{-6}[J(J+1)]^2$	0.5	4.0(4)	4.0(4)		1.9

[a] This work; constants derived using the modeling procedure described in the text. Constants for the 12,0 band were determined by fitting the region 31 220−31 470 cm^{-1}. [b] Uncertainty from the fit for the ^{79}BrO and ^{81}BrO constants determined in this work. [c] Values taken from Wheeler et al.[23] [d] Values taken from Barnett et al.[21] Numbers in parentheses are the uncertainties as listed in the references. [e] Value fixed at that obtained for the 12,0 band of ^{81}BrO.

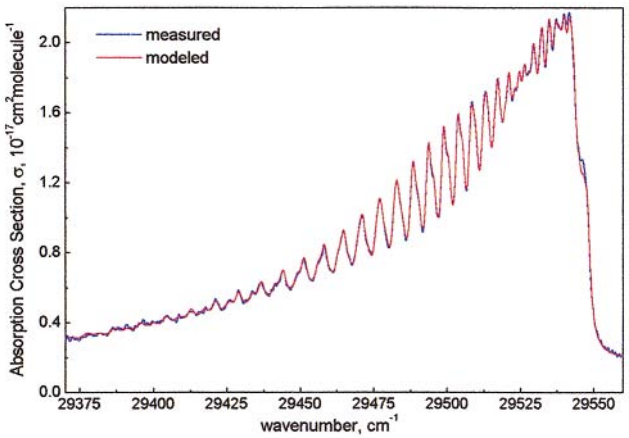

Figure 4. 1.0 cm^{-1} resolution UV absorption spectrum of the A $^2\Pi_{3/2} \leftarrow$ X $^2\Pi_{3/2}$ 7,0 band of BrO at 298 ± 2 K. The modeled 7,0 spectrum, shown overlaying the measured spectrum, was produced using the method described in the text.

resolution with no apodization. There is no loss of structure in degrading to 1.0 cm^{-1}. Cross sections were assigned using a technique similar to that described for the vibrational transitions. The resolution of the band was degraded, and the 7,0 absorption cross sections determined in Table 1 were used as the reference for determining the multiplicative factor and additive factor to apply to the absorption spectrum of the band. The cross section at the apex of the high-resolution 7,0 band is 2.17×10^{-17} cm^2 molecule^{-1} at 29 541.5 cm^{-1}.

Spectroscopic constants for the BrO 7,0 band were determined from a least squares comparison of modeled and measured spectra. A description of the model follows, with more specific details in the Appendix. Modeled line positions were calculated for the P, Q, and R branches using the standard formulas, including the correction for centrifugal distortion. Line intensities for each branch were found by normalizing the product of the *J*-state population and the appropriate Hönl−London factor. The linewidth for BrO is dominated by lifetime broadening, and linewidths were modeled with various *J* dependences in order to determine the best match. Using the line position, intensity, and linewidth information, each peak was simulated with a Lorentzian line profile. Because of the large natural abundance of two bromine isotopes (50.69% ^{79}Br, 49.31% ^{81}Br) the positions, intensities, and linewidths were modeled independently for the two isotopomers of BrO. The modeled spectrum was normalized to the measured spectrum using a multiplicative factor and an additive factor, and the baseline influences of the neighboring 6,0 and 8,0 bands and the $v'' = 1$ hotband were incorporated.

Spectroscopic constants for the BrO ground state were taken from the literature.[33] Excited-state constants determined from the model were used to create the simulated 7,0 rotational spectrum in Figure 4. The modeled spectrum is shown overlaying the measured spectrum so that direct comparison is possible. The overall shape of the band contour is reproduced by the simulated spectrum, as are the individual rotational peaks. Modeling was complicated by the fact that each peak in the spectrum is actually a convolution of a number of rotational peaks. Overlapping P and R branches of both isotopomers plus the weak Q branches convolve to form the overall 7,0 rotational band structure. The source of the spectral "shoulders", seen in the measured spectrum at around 29 460, 29 500, and 29 550 cm^{-1}, is thus explained by the convolution of the spectral branches.

The A-state molecular constants of BrO determined from the model are listed in Table 3. ^{79}BrO and ^{81}BrO band origins, rotational constants, centrifugal distortion constants, and fwhm linewidths are presented. Uncertainty from the fit, as well as the previous literature values, are shown. In order that our theoretical spectra may be accurately reproduced, some values determined in this work are presented with more significant figures than are justified by their uncertainties.[51] Blank entries in the table indicate constants not determined in the previous studies. The *D* values from this work were modeled independently for both isotopomers but could not be distinguished within the fit uncertainty. In particular, the BrO linewidths exhibit a *J* dependence, increasing as $[J(J+1)] + [J(J+1)]^2$ with multipliers for each term determined in the model. The linewidth variation with excited-state rotational level is shown in the top panel of Figure 5. The linewidths are approximately 2.0 cm^{-1} at the lowest *J* state and broaden as *J* increases. Predissociative lifetimes corresponding to the linewidths are also shown in the upper panel of Figure 5. At the lowest excited *J* level the natural lifetime is a maximum of 2.5 ± 0.2 ps for ^{79}BrO and 2.7 ± 0.2 ps for ^{81}BrO. As *J* increases, the lifetimes decrease. The range of *J* levels plotted corresponds to that required to cover the wavenumber range in Figure 4 for all of the convolved spectral branches.

12,0 Band. The ambient temperature (298 ± 2 K) rotational spectrum of the 12,0 band is shown in Figure 6. The spectrum was acquired at 0.5 cm^{-1} resolution and is shown here degraded to 1.5 cm^{-1} resolution with no apodization. As with the 7,0 band, no structure is lost in the degradation. Cross sections were assigned by referencing to the 12,0 cross section of the vibrational spectrum determined in this work. The cross section at the apex of the high-resolution 12,0 band is 1.38×10^{-17} cm^2 molecule^{-1} at 31 530.3 cm^{-1}.

Modeling of the 12,0 band was done in a manner analogous to that for the 7,0 band. Excited-state constants determined in this work, along with literature values[33] for the BrO ground

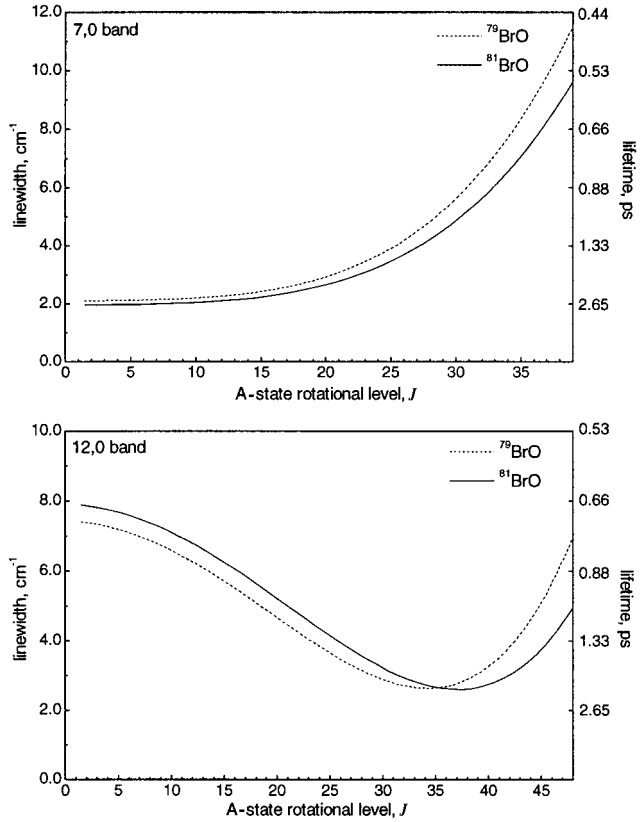

Figure 5. (Top) Modeled 7,0 band linewidths and predissociative lifetimes as a function of excited-state rotational level for ^{79}BrO and ^{81}BrO. (Bottom) Modeled 12,0 band linewidths and predissociative lifetimes as a function of excited-state rotational level for ^{79}BrO and ^{81}BrO. Linewidths change with J according to the equations in Table 3.

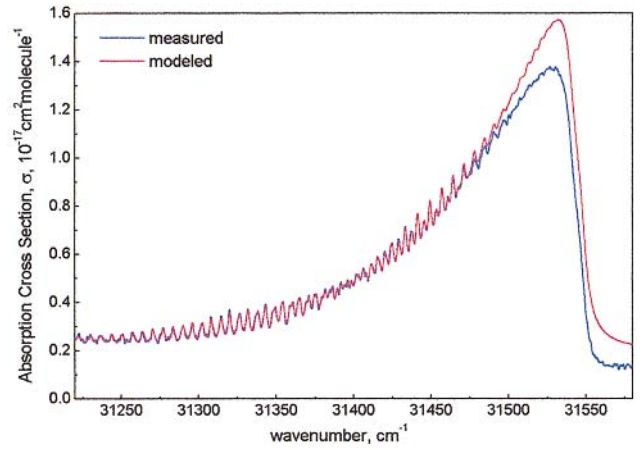

Figure 6. 1.5 cm^{-1} resolution UV absorption spectrum of the A $^2\Pi_{3/2}$ ← X $^2\Pi_{3/2}$ 12,0 band of BrO at 298 ± 2 K. The modeled 12,0 spectrum, shown overlaying the measured spectrum, was produced by fitting to the spectral region 31 220−31 470 cm^{-1} using the method described in the text.

state, produce the simulated 12,0 spectrum shown overlaying the measured spectrum in Figure 6. A number of different spectral regions with various starting parameters were used in attempts to model this band, but simultaneous reproduction of the individual rotational peaks and the overall band contour of the measured spectrum was not possible. The spectrum shown here was produced by fitting to the region 31 220−31 470 cm^{-1}. This wavenumber range represents most of the resolvable rotational structure and is reproduced well by the model. Overlapping P, Q, and R branches of ^{79}BrO and ^{81}BrO convolve to form the overall rotational structure for the 12,0 band.

The A-state molecular constants determined from modeling the region 31220−31470 cm^{-1} are listed in Table 3. The D values were fit independently for the two isotopomers but could not be distinguished within the fit uncertainty. Uncertainties for the 12,0 constants are generally larger than for the 7,0 due to lower signal-to-noise in the measured spectrum and greater difficulty in modeling. The linewidths for the 12,0 band also exhibit a J dependence, changing as $[J(J+1)] + [J(J+1)]^2$ with multipliers for each term determined in the model. As shown in the lower panel of Figure 5, the linewidths decrease as J increases, reach a minimum value around 2.6 cm^{-1} for both isotopomers, and then increase as J increases. Predissociative lifetimes corresponding to the linewidths are also shown in the lower panel of Figure 5. The natural lifetime at the linewidth minima is 2.0 ± 0.5 ps and decreases at both higher and lower excited J values. The range of J levels plotted corresponds to that required to cover the wavenumber range in Figure 6 for all of the convolved spectral branches. Linewidth and lifetime values are plotted using the results of modeling the region 31 220−31 470 cm^{-1}. Values at low J, i.e., high wavenumbers, are shown for completeness but have large uncertainties.

Discussion

A. Vibrational Data. *Spectra.* Since the Wahner et al.[31] BrO spectra have been an important reference used in atmospheric studies for some time, it is of interest here to compare the 298 ± 2 K BrO spectrum from this work with that from Wahner et al.[31] The spectra are shown in Figure 7. Our experimental spectrum is presented at 35 cm^{-1} resolution as in Figure 2, while the Wahner et al.[31] spectrum is at 0.40 nm resolution. As was indicated previously, the BrO spectrum is resolution dependent, and it is important to note that only at the 7,0 peak does the 35 cm^{-1} spectrum exactly correspond to 0.40 nm. However, the resolution difference between the two spectra is quite small at most of the other bands (e.g., at the 4,0 band 35 cm^{-1} corresponds to 0.44 nm resolution, and at the 12,0 band 35 cm^{-1} is 0.35 nm resolution); therefore general spectral comparison is possible.

While the same basic band structure is present for both spectra in Figure 7, the two differ significantly. The Wahner et al.[31] spectrum is shifted to higher wavenumbers relative to our spectrum. At the 7,0 band this offset is 33 cm^{-1}. The offset between the spectra, however, is not simply due to an absolute shift. The inset in Figure 7 shows the 4,0−7,0 bands from this work replotted with the Wahner et al.[31] spectrum wavenumber normalized to our 7,0 band, i.e., minus 33 cm^{-1}. After the subtraction, the 4,0 and 5,0 bands of the Wahner et al.[31] spectrum are red-shifted by 16 and 6 cm^{-1} respectively, and the 6,0 band is blue-shifted by 2 cm^{-1} relative to our spectrum. All shifts are determined at the half-maximum point on the higher wavenumber side of the band. Clearly, there is not an easily corrected constant offset between the spectra.

The baselines of the two spectra are also significantly different. The baseline of the Wahner et al.[31] spectrum rises to much higher levels in the neighborhood of the 7,0 band and then falls off abruptly at the 12,0 and 13,0 peaks. Relative cross sections differ for the two spectra as well. For instance, the percent difference in the differential cross sections of the 7,0 bands is approximately 2.5 times that of the 4,0 bands; i.e., a constant multiplier will not normalize the spectra. Comparisons of our low-temperature spectrum with that from Wahner et al.[31]

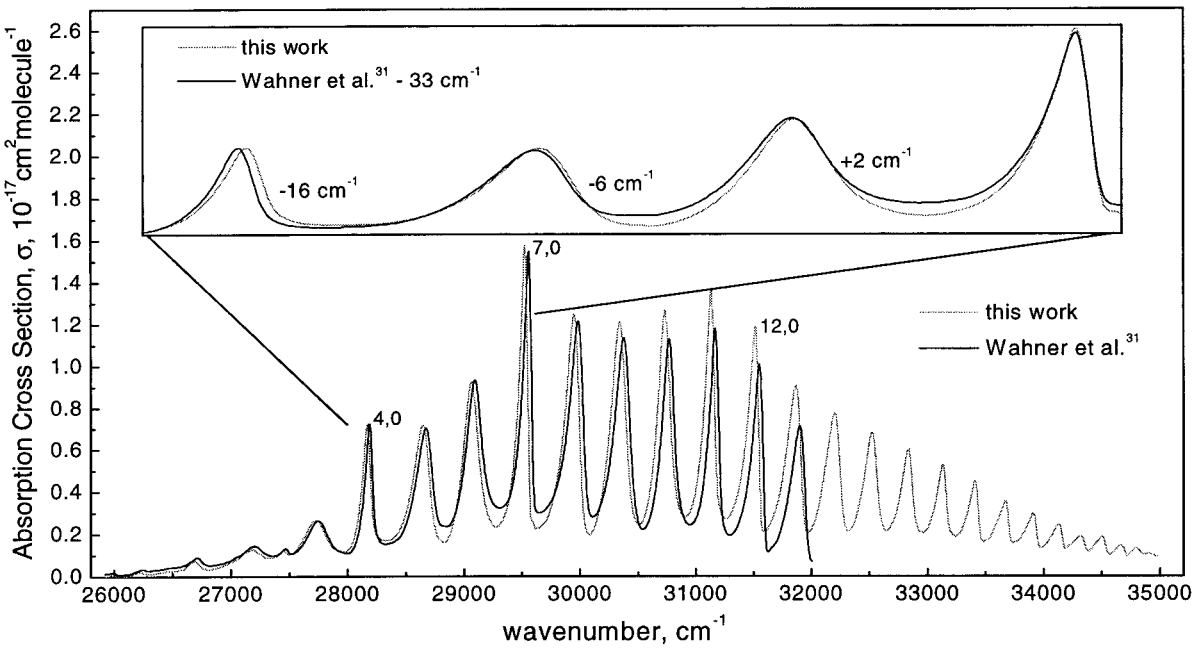

Figure 7. 35 cm^{-1} resolution UV absorption spectrum of BrO from this work overlaid with the 0.40 nm resolution Wahner et al.[31] spectrum. Both spectra are at 298 ± 2 K. (Inset) The 4,0−7,0 bands from this work replotted with the Wahner et al.[31] spectrum minus 33 cm^{-1}.

yield discrepancies similar to those described for the ambient temperature spectra.

The exact cause of these discrepancies is not clear. For certain, highly accurate wavelength calibration was not an objective of the Wahner et al.[31] work. Perhaps the most significant difference in the studies is simply the spectroscopic technique used in acquiring the spectra. The advantages of Fourier transform spectroscopy over dispersive spectroscopy have been well-documented. In particular, the FT technique provides spectra of higher accuracy in wavenumber positions and relative cross sections.

Cross Sections. There are currently differences in the literature regarding which BrO reference cross sections are used for analysis, with most researchers using either the Wahner et al.[31] or the recent Gilles et al.[26] study. However, there is no clear reason to discount any of the five cross section studies in Table 1. Thus, we assign cross sections to our spectra on the basis of all the data. Although it should be noted that the absolute cross section of Orlando et al.[33] has a larger uncertainty than the other values since it was determined indirectly on the basis of calculated infrared intensities. The resulting values provide cross sections representative of a number of literature studies and should be more reliable than using the results of any single study. For the bands most commonly used in atmospheric measurements (4,0−7,0), we find an uncertainty of 8% for the absolute cross section and 11% for the differential based on the variance in the literature 7,0 band cross sections. From the temperature dependence data there is a negligible additional uncertainty in determining the 228 K cross sections from those at 298 K, so we assign the same uncertainties to the low-temperature spectrum.

While there is no evident justification for eliminating certain studies from our analysis, it is interesting to note that removing the highest (Gilles et al.[26]) and lowest (Orlando et al.[33]) values from the absolute cross section calculation in Table 1 yields the same average 7,0 band absolute cross section, but with a variance of only 1.7% instead of 8%. Regardless of the absolute or differential cross sections assigned, the accuracy of the relative cross sections of the vibrational bands in our spectra is not affected.

TABLE 4: Heats of Formation of BrO(g) in kJ/mol

ref	$\Delta_f H°$(298 K)	$\Delta_f H°$(0 K)
36	125.8 ± 2.4	133.3 ± 2.4
37	119.7 ± 5.9	
38	119.2 ± 4.2	
this work	126.2 ± 1.7	133.7 ± 1.7

Dissociation Energy and Heat of Formation. There have been two previous experimental spectroscopic studies that yielded dissociation energies for BrO(g). Coleman and Gaydon[29] recommended a ground-state dissociation energy of 14 240 cm^{-1} following a long Birge−Sponer extrapolation of the ground-state vibrational intervals. Durie and Ramsay,[22] using their BrO $A \leftarrow X$ spectrum, determined the dissociation energy from a graphical Birge−Sponer extrapolation and by extrapolating an equation representing the band heads. The limit was determined to be ∼35 200 cm^{-1} with an estimated uncertainty of ±200 cm^{-1}. Subtracting the $^1D_2-^3P_2$ excitation energy of the oxygen atom yields 19 332 ± 200 cm^{-1} for the ground-state dissociation energy. Our $A \leftarrow X$ dissociation energy of 35 180 ± 140 cm^{-1} and ground-state dissociation energy of 19 312 ± 140 cm^{-1} are in good agreement with the results of Durie and Ramsay.[22] Our values fall within their uncertainty range but are of improved accuracy since we observe three higher v' bands and can hence better constrain the extrapolation to the dissociation limit.

The heat of formation of BrO(g) has been determined a number of times but with considerable uncertainty. The values recommended in the NIST-JANAF Thermochemical Tables[36] were determined using the ground-state dissociation energy of Durie and Ramsay.[22] These values are listed in Table 4. Also in Table 4 are recently determined values for the heat of formation of BrO in kinetic studies by Bedjanian et al.[37] and Gilles et al.[38] Our heats of formation agree well with the NIST-JANAF values and have an overlapping uncertainty range with Bedjanian et al.[37] at 298 K. However, there is clearly a discrepancy in the results from the spectroscopic data and the kinetic data.

The only significant source of uncertainty in the calculation of BrO(g) heats of formation from the spectroscopic data is the dissociation energy uncertainty. Calculating the implied dis-

sociation energies from the heats of formation proposed by Bedjanian et al.[37] and Gilles et al.[38] yields values approximately 420 cm^{-1} higher (and as much as 900 cm^{-1} higher within their uncertainty limit) than the upper bound on the dissociation energy determined in this work. This would require the Birge−Sponer plot of BrO to have anomalous positive curvature, i.e., an abrupt upward inflection, near the dissociation limit. Though this is unlikely, the lack of observed peaks near the dissociation limit prevents us from eliminating this possibility.

Inaccuracies in the heats of formation from kinetic studies can originate from rate constant values. However, the rate constants need not necessarily be inaccurate in order to explain the $\Delta_f H°$ discrepancy with the spectroscopic data for BrO. Rather, the more likely source of uncertainty in the kinetic studies appears to be from the indirect way in which the heat of formation is calculated. Specifically, Bedjanian et al.[37] found the heat of formation of BrO relative to that of IO. The heat of formation of IO, however, is poorly known with a recommended uncertainty range of ±18 kJ/mol.[36] The $\Delta_f H°$(IO) used by Bedjanian et al.[37] was derived relative to that of OClO[52] and is ~10 kJ/mol lower than the value derived by averaging the dissociation energies from two molecular beam studies.[53] Gilles et al.[38] also used the heat of formation of OClO in order to find the heat of formation of BrO. As mentioned by Bedjanian et al.,[37] a new accurate measurement of $\Delta_f H°$(OClO) or $\Delta_f H°$(IO) would be beneficial in reducing the uncertainty on the kinetically determined $\Delta_f H°$(BrO). Such a measurement could perhaps help ameliorate the discrepancy in the spectroscopic and kinetic $\Delta_f H°$(BrO) values.

B. Rotational Data. One of the motivations for this work was to determine whether individual rotational peaks of each branch of the 7,0 and 12,0 bands could be resolved at very high resolution and whether these peaks might exhibit much larger absolute and differential cross sections that could be used to identify BrO in the atmosphere. To this end, we acquired spectra at higher resolution than those presented here but never observed the deconvolution of peaks beyond the levels presented in Figures 4 and 6. The cross sections for the 7,0 and 12,0 rotational peaks in Figures 4 and 6 are the first to be reported. Our band head values represent the highest resolution vibrational peak cross sections obtained and should place an upper limit on the resolution-dependent absolute cross sections for the 7,0 and 12,0 bands at 298 K.

In our model, spectroscopic constants were fit independently for the two isotopomers of BrO. One initial test to check the validity of our revised rotational constants is whether the ratio $B(^{79}BrO)/B(^{81}BrO)$ is equal to the ratio of the reduced masses $\mu(^{81}BrO)/\mu(^{79}BrO) = 1.0042$. These ratios must be equal in order for the B values to be physically acceptable. Checking our rotational constants, shown in Table 3, against this criterion yields remarkable agreement. Our B value ratios for both the 7,0 and 12,0 bands agree with the reduced mass ratios to within 0.004%.

7,0 Band. Comparison of the molecular constants of the 7,0 band from this work with the previous literature yields mixed results, as shown in Table 3. Our band origins are slightly lower in energy than those of Wheeler et al.,[23] but we confirm their relatively large upward shift of the band origins from the original values of Barnett et al.[21] The rotational constant differences between the studies are small, but significant. Even a seemingly small B value change can have a large impact on the modeled spectrum. Our centrifugal distortion constants for the 7,0 peak are the first to be directly determined. We observe J-dependent linewidths, while the values from the earlier work are constant at all rotational levels.

To some degree we expect our molecular constants to differ from those in previous studies. Our spectrum has high wavenumber accuracy and exhibits improved signal-to-noise relative to earlier spectra. Having a high signal-to-noise ratio is especially important for detecting the spectral shoulders and adjusting the modeled constants in order to reproduce them. Differing model content, e.g., including centrifugal distortion values and considering J-dependent linewidths, is another reason our molecular constants will not necessarily agree with the earlier work. Covariance between molecular constants in the model can cause one differently modeled variable to affect the values of all the other modeled variables. For instance, our B value discrepancy with Wheeler et al.[23] is at least partly caused by their modeling of BrO as a rigid rotor. Neglecting the centrifugal distortion correction results in lowering the predicted B value.

A comparison of modeled spectra is useful for evaluating the molecular constants. The Barnett et al.[21] data have previously been discussed,[23] so we focus here on relating our data to those of Wheeler et al.[23] The 7,0 band modeled using the constants from this work and from Wheeler et al.[23] is shown in Figure 8. The upper and middle panels display the modeled spectra overlaying our measured spectrum in a close-up view of the structured region of the band. The spectrum using the Wheeler et al.[23] constants was produced by using our model to optimize the normalization to our measured spectrum. The residuals of the modeled spectra relative to the measured one are shown in the lowermost panel of Figure 8. The spectra and the residuals indicate that our molecular constants better reproduce the experimental 7,0 band spectrum. What appears as an intensity offset in much of the spectrum using the Wheeler et al.[23] constants is actually primarily a manifestation of their J-independent linewidth. Modeled linewidths that are too broad have too little intensity, and linewidths that are too narrow overpredict the peak intensity.

The A state of BrO is extensively predissociated. We interpret the broadening 7,0 band linewidths to mean that an avoided curve crossing is being approached at successively higher excited J levels. As the curve crossing gets closer, the natural lifetimes shorten and the linewidths increase, as seen in the upper panel of Figure 5.

12,0 Band. As discussed for the 7,0 band, we expect some differences in the 12,0 modeled constants from this work and those from previous studies due to differences in measured spectra and model content. Our band origins are slightly lower in energy than those of Barnett et al.[21] but agree well relative to the significantly smaller values of Wheeler et al.[23] The B values from all studies are in agreement within our fit uncertainty. Our centrifugal distortion constants agree with those of Barnett et al.,[21] who determined the D value of ^{81}BrO directly and then used that number for ^{79}BrO. The linewidths again differ among the studies, as we observe J-dependent linewidths, while the previously reported values are constant at all J states.

A comparison of the 12,0 band modeled using our constants and those from Wheeler et al.[23] is shown in Figure 9. The upper and middle panels display the modeled spectra overlaying our measured spectrum in the region 31 220−31 470 cm^{-1}. The spectrum using the Wheeler et al.[23] constants was produced by using our model to optimize the normalization to our measured spectrum. The residuals of the modeled spectra relative to the measured one are shown in the lowermost panel of Figure 9. The spectra and residuals indicate that our molecular constants

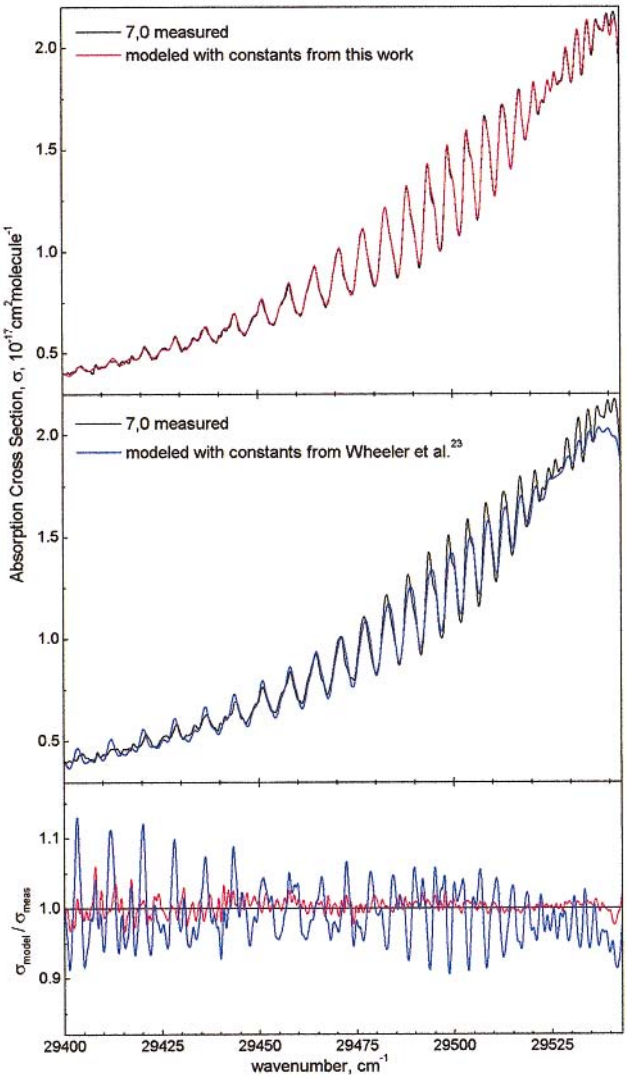

Figure 8. (Top) Close-up view of the 7,0 band spectrum modeled using the constants from this work overlaying the measured spectrum from this work. (Middle) Close-up view of the 7,0 band spectrum modeled using the constants from Wheeler et al.[23] overlaying the measured spectrum from this work. (Bottom) Residual plots of the modeled/measured spectra. The legend is the same as in the upper panels.

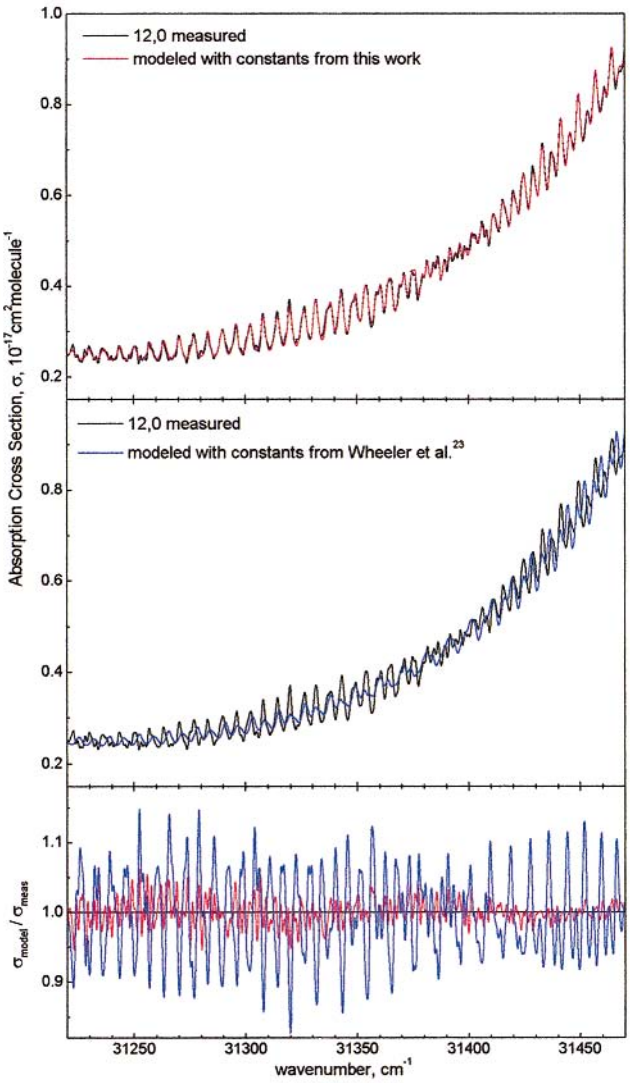

Figure 9. (Top) Close-up view of the 12,0 band spectrum modeled using the constants from this work overlaying the measured spectrum from this work. (Middle) Close-up view of the 12,0 band spectrum modeled using the constants from Wheeler et al.[23] overlaying the measured spectrum from this work. (Bottom) Residual plots of the modeled/measured spectra. The legend is the same as in the upper panels.

better reproduce the experimental 12,0 band spectrum. In particular, using the Wheeler et al.[23] constants, there is significant offset in many of the peak locations and peak intensities relative to those measured. Differences in the wavenumber positions of our measured spectrum with those of Wheeler et al.,[23] as indicated by the discrepancy in band origins, as well as the differently modeled linewidths are primarily responsible.

As with the 7,0 band, we interpret the *J* dependence of the 12,0 band linewidths to be the result of interactions of other electronic states with the BrO A state. The 12,0 band is apparently positioned such that as the excited-state *J* levels increase, an avoided curve crossing from below is being distanced and one above is being approached. The linewidth minimum, i.e., natural lifetime maximum, corresponds to the excited *J* state where these curve crossings have the least influence. This occurs in the neighborhood of 31 350 cm^{-1}, depending on the BrO branch and isotopomer.

While our model accurately reproduces the 12,0 band spectral features in the region 31 220−31 470 cm^{-1}, the agreement at higher wavenumbers is much worse, as shown in Figure 6. Even though there is a large intensity disagreement, the model does exhibit the correct peak structure and then the transition to lack of structure at around 31 500 cm^{-1} just as in the measured spectrum. A simple baseline translation is not sufficient to reproduce this spectral region, however, since the simulated spectrum is more intense at the band head even when shifted downward. We attempted numerous model runs, but this region of the 12,0 spectrum could not be fit while simultaneously reproducing the individual rotational peak structure.

Potential sources of the difference between the modeled and measured spectra at wavenumbers higher than 31 470 cm^{-1} were considered. A chemical impurity or baseline artifact could theoretically cause the discrepancy, but since our sample spectra are referenced to background spectra, most such influences will divide out. Analysis of our background and sample spectra showed no evidence that the peak intensities of the measured 12,0 band spectrum should not be accurate. A significant hotband component is another possible means to explain the modeled and measured spectra offset. The 14,1 hotband is

directly underneath the 12,0 band with its band head at around 31 480 cm^{-1}. A very large contribution from this band would aid greatly in our ability to reproduce the region of peak structure, while also lowering the baseline at the higher wavenumbers. However, there does not appear to be justification for including a large hot component. Also, even if the size of the 14,1 hotband is allowed to float as a free parameter in the model, the simulated spectrum is improved but still not accurate at the higher wavenumbers. To eliminate any baseline influences in our fitting procedure, we modeled the interferogram of the 12,0 spectrum in addition to the spectrum itself. This, however, yielded the same results as those from just fitting the absorption spectrum.

We conclude that the discrepancy between our measured and modeled 12,0 spectra is due to a real phenomenon affecting the high wavenumber peaks. The A state of the 12,0 band is apparently particularly perturbed at the lowest J levels. A perturbation that alters any of the predicted values, such as line shapes, linewidths, B values, or peak intensities could contribute to the discrepancy. Although not mentioned in previous studies, it appears that difficulties in reproducing the overall shape of the 12,0 band have been encountered before. Wheeler et al.[23] presented their modeled and measured spectra offset from one another, but overlaying them reveals similar band contours to those presented in this work. This provides further evidence that the whole 12,0 band cannot simultaneously be modeled with just one set of molecular constants.

At present no ab initio calculations regarding the positioning of BrO excited states have been reported. Most of the A $^2\Pi_{3/2} \leftarrow$ X $^2\Pi_{3/2}$ bands are completely diffuse, and those bands that do exhibit structure are significantly perturbed. However, very little is actually known about the mechanisms that are responsible. It is in fact feasible that numerous potentials could perturb the A state causing the observed diffuse band structure.[23] Clearly, there is a need for ab initio calculations in this area.

Conclusions

We obtain spectra of the A $^2\Pi_{3/2} \leftarrow$ X $^2\Pi_{3/2}$ electronic transition of BrO using Fourier transform ultraviolet spectroscopy. Vibrational spectra acquired at 298 ± 2 K and 228 ± 5 K have highly accurate wavenumbers and relative cross sections. Absolute and differential cross sections from previous studies are converted to a common resolution for direct comparison, and the data are used to assign representative cross section values to our spectra. These vibrational spectra should prove particularly useful in analyzing GOME data.

BrO dissociation energies are determined from a graphical Birge−Sponer extrapolation. The upper bound on the dissociation limit is determined by assuming positive curvature appears on the Birge−Sponer plot immediately following our last observed data point, and Le Roy−Bernstein theory is used to guide the extrapolation. Heats of formation of BrO(g) at 0 and 298 K are derived from the ground-state dissociation energy.

High-resolution rotational spectra of the 7,0 and 12,0 vibrational bands are obtained. Cross sections for the rotational peaks are reported for the first time. Modeling the bands yields improved band origins, rotational constants, centrifugal distortion constants, linewidths, and lifetimes. In particular, we observe J-dependent linewidths for both vibrational peaks and find that the entire 12,0 band cannot be modeled with just one set of molecular constants.

Acknowledgments. We thank Kelly Chance and Paul Wennberg for helping to provide the motivation for this work. We gratefully acknowledge Andreas Wahner for granting us permission to include his BrO spectrum in Figure 7. Support for the purchase of the Bruker FTS was provided through grants from the National Science Foundation (ATM-8921312), the Empire State Electrical Energy Research Corporation, and the Electric Power Research Institute. Additional support was provided by the NASA Upper Atmosphere Research Program (NAG-1-1305). D.M.W. acknowledges support from a National Defense Science and Engineering Graduate Fellowship.

Appendix

Modeled line positions were determined by calculating the energy of the P, Q, and R branches for each rotational level, J, according to

$$\nu_P(J) = \nu_0 + E_A(J-1) - E_X(J)$$

$$\nu_Q(J) = \nu_0 + E_A(J) - E_X(J)$$

$$\nu_R(J) = \nu_0 + E_A(J+1) - E_X(J)$$

where ν_P, ν_Q, and ν_R are the transition energies as a function of J, and ν_0 is the band origin. E_A and E_X are the J-dependent term values for the BrO excited and ground states, respectively, calculated as

$$E(J) = BJ[J+1] - D[J(J+1)]^2$$

where B is the rotational constant and D is the centrifugal distortion constant for each electronic state.

Modeled line intensities were found by normalizing the product of the population and the respective Hönl-London factor for each J level. The J-state population, P_J, is calculated as

$$P_J = [2J+1]e^{-E_x/kT}/q_r$$

where k is the Boltzmann constant, T is temperature, and q_r is the partition function,

$$q_r = \sum [2J+1]e^{-E_x/kT}$$

Hönl−London factors, i.e., rotational line strength terms, depend on the electronic transition involved. For a $\Pi \leftarrow \Pi$ transition, where $\Delta\Lambda = 0$ and $\Lambda = 1$, the Hönl−London factors for each rotational branch are[54]

$$S_J^P = [J+1][J-1]/J$$

$$S_J^Q = [2J+1]/J[J+1]$$

$$S_J^R = J[J+2]/[J+1]$$

Linewidths were modeled as various functions of J. The representation of the measured spectra was achieved by modeling fwhm linewidths for the P, Q, and R branches as

$$\text{linewidth} = \alpha + \beta J[J+1] + \gamma[J(J+1)]^2$$

where α, β, and γ are values determined in the model.

References and Notes

(1) Wofsy, S. C.; McElroy, M. B.; Yung, Y. L. *Geophys. Res. Lett.* **1975**, *2*, 215.

(2) McElroy, M. B.; Salawitch, R. J.; Wofsy, S. C.; Logan, J. A. *Nature* **1986**, *321*, 759.

(3) Anderson, J. G.; Brune, W. H.; Lloyd, S. A.; Toohey, D. W.; Sander, S. P.; Starr, W. L.; Loewenstein, M.; Podolske, J. R. *J. Geophys. Res.* **1989**, *94*, 11480.

(4) Garcia, R. R.; Solomon, S. *J. Geophys. Res.* **1994**, *99*, 12937.
(5) Wennberg, P. O.; Cohen, R. C.; Stimpfle, R. M.; Koplow, J. P.; Anderson, J. G.; Salawitch, R. J.; Fahey, D. W.; Woodbridge, E. L.; Keim, E. R.; Gao, R. S.; Webster, C. R.; May, R. D.; Toohey, D. W.; Avallone, L. M.; Proffitt, M. H.; Loewenstein, M.; Podolske, J. R.; Chan, K. R.; Wofsy, S. C. *Science* **1994**, *266*, 398.
(6) Hausmann, M.; Platt, U. *J. Geophys. Res.* **1994**, *99*, 25399.
(7) Lary, D. J. *J. Geophys. Res.* **1996**, *101*, 1505.
(8) Wamsley, P. R.; Elkins, J. W.; Fahey, D. W.; Dutton, G. S.; Volk, C. M.; Myers, R. C.; Montzka, S. A.; Butler, J. H.; Clarke, A. D.; Fraser, P. J.; Steele, L. P.; Lucarelli, M. P.; Atlas, E. L.; Schauffler, S. M.; Blake, D. R.; Rowland, F. S.; Sturges, W. T.; Lee, J. M.; Penkett, S. A.; Engel, A.; Stimpfle, R. M.; Chan, K. R.; Weisenstein, D. K.; Ko, M. K. W.; Salawitch, R. J. *J. Geophys. Res.* **1998**, *103*, 1513.
(9) World Meteorological Organization (WMO), *Scientific Assessment of Ozone Depletion: 1994*; WMO Global Ozone Research and Monitoring Project, Report 37, Geneva, Switzerland, 1994.
(10) Solomon, S.; Sanders, R. W.; Carroll, M. A.; Schmeltekopf, A. L. *J. Geophys. Res.* **1989**, *94*, 11393.
(11) Carroll, M. A.; Sanders, R. W.; Solomon, S.; Schmeltekopf, A. L. *J. Geophys. Res.* **1989**, *94*, 16633.
(12) Wahner, A.; Schiller, C. *J. Geophys. Res.* **1992**, *97*, 8047.
(13) Arpag, K. H.; Johnston, P. V.; Miller, H. L.; Sanders, R. W.; Solomon, S. *J. Geophys. Res.* **1994**, *99*, 8175.
(14) Kreher, K.; Johnston, P. V.; Wood, S. W.; Nardi, B.; Platt, U. *Geophys. Res. Lett.* **1997**, *24*, 3021.
(15) Aliwell, S. R.; Jones, R. L.; Fish, D. J. *Geophys. Res. Lett.* **1997**, *24*, 1195.
(16) Richter, A.; Wittrock, F.; Eisinger, M.; Burrows, J. P. *Geophys. Res. Lett.* **1998**, *25*, 2683.
(17) Hegels, E.; Crutzen, P. J.; Klüpfel, T.; Perner, D.; Burrows, J. P. *Geophys. Res. Lett.* **1998**, *25*, 3127.
(18) Chance, K. *Geophys. Res. Lett.* **1998**, *25*, 3335.
(19) Wagner, T.; Platt, U. *Nature* **1998**, *395*, 486.
(20) Ferlemann, F.; Camy-Peyret, C.; Fitzenberger, R.; Harder, H.; Hawat, T.; Osterkamp, H.; Schneider, M.; Perner, D.; Platt, U.; Vradelis, P.; Pfeilsticker, K. *Geophys. Res. Lett.* **1998**, *25*, 3847.
(21) Barnett, M.; Cohen, E. A.; Ramsay, D. A. *Can. J. Phys.* **1981**, *59*, 1908.
(22) Durie, R. A.; Ramsay, D. A. *Can. J. Phys.* **1958**, *36*, 35.
(23) Wheeler, M. D.; Newman, S. M.; Ishiwata, T.; Kawasaki, M.; Orr-Ewing, A. J. *Chem. Phys. Lett.* **1998**, *285*, 346.
(24) Cox, R. A.; Sheppard, D. W.; Stevens, M. P. *J. Photochem.* **1982**, *19*, 189.
(25) Sander, S. P.; Watson, R. T. *J. Phys. Chem.* **1981**, *85*, 4000.
(26) Gilles, M. K.; Turnipseed, A. A.; Burkholder, J. B.; Ravishankara, A. R.; Solomon, S. *J. Phys. Chem. A* **1997**, *101*, 5526.
(27) Harwood: M. H.; Rowley, D. M.; Cox, R. A.; Jones, R. L. *J. Phys. Chem. A* **1998**, *102*, 1790.
(28) Vaidya, W. M. *Proc. Indian Acad. Sci.* **1938**, *A 7*, 321.
(29) Coleman, E. H.; Gaydon, A. G. *Discuss. Faraday Soc.* **1947**, *2*, 166.
(30) Loewenschuss, A.; Miller, J. C.; Andrews, L. *J. Mol. Spectrosc.* **1980**, *81*, 351.
(31) Wahner, A.; Ravishankara, A. R.; Sander, S. P.; Friedl, R. R. *Chem. Phys. Lett.* **1988**, *152*, 507.
(32) DeMore, W. B.; Sander, S. P.; Golden, D. M.; Hampson, R. F.; Kurylo, M. J.; Howard, C. J.; Ravishankara, A. R.; Kolb, C. E.; Molina, M. J. *Chemical Kinetics and Photochemical Data for Use in Stratospheric Modeling*; JPL publication 97-4; California Institute of Technology: Pasadena, 1997.
(33) Orlando, J. J.; Burkholder, J. B.; Bopegedera, A. M. R. P.; Howard, C. J. *J. Mol. Spectrosc.* **1991**, *145*, 278.
(34) Laszlo, B.; Huie, R. E.; Kurylo, M. J.; Miziolek, A. W. *J. Geophys. Res.* **1997**, *102*, 1523.
(35) Harder, J. W.; Brault, J. W.; Johnston, P. V.; Mount, G. H. *J. Geophys. Res.* **1997**, *102*, 3861.
(36) Chase, M. W., Jr. *J. Phys. Chem. Ref. Data*, *Monograph 9* **1998**.
(37) Bedjanian, Y.; Le Bras, G.; Poulet, G. *Chem. Phys. Lett.* **1997**, *266*, 233.
(38) Gilles, M. K.; Turnipseed, A. A.; Burkholder, J. B.; Ravishankara, A. R. *Chem. Phys. Lett.* **1997**, *272*, 75.
(39) Chase, M. W., Jr. *J. Phys. Chem. Ref. Data* **1996**, *25*, 1069.
(40) Wennberg, P. O.; Brault, J. W.; Hanisco, T. F.; Salawitch, R. J.; Mount, G. H. *J. Geophys. Res.* **1997**, *102*, 8887.
(41) Gerstenkorn, S.; Luc, P. *Rev. Phys. Appl.* **1979**, *14*, 791.
(42) Douglas, A. E.; Møller, Chr. Kn.; Stoicheff, B. P. *Can. J. Phys.* **1963**, *41*, 1, 1174.
(43) Le Roy, R. J.; Bernstein, R. B. *J. Mol. Spectrosc.* **1971**, *37*, 109.
(44) Brown, W. G. *Phys. Rev.* **1931**, *38*, 1179.
(45) Brown, W. G. *Phys. Rev.* **1931**, *38*, 709.
(46) Coxon, J. A.; Ramsay, D. A. *Can. J. Phys.* **1976**, *54*, 1034.
(47) Gaydon, A. G. *Dissociation Energies and Spectra of Diatomic Molecules*, 3rd ed.; Chapman and Hall: London, 1968.
(48) Le Roy, R. J.; Bernstein, R. B. *Chem. Phys. Lett.* **1970**, *5*, 42.
(49) Le Roy, R. J.; Bernstein, R. B. *J. Chem. Phys.* **1970**, *52*, 3869.
(50) Le Roy, R. J. In *Molecular Spectroscopy*; Specialist Periodical Report; The Chemical Society: London, 1973; Vol. I, p 113.
(51) Watson, J. K. G. *J. Mol. Spectrosc.* **1977**, *66*, 500.
(52) Bedjanian, Y.; Le Bras, G.; Poulet, G. *J. Phys. Chem. A* **1997**, *101*, 4088.
(53) Zhang, Z.; Monks, P. S.; Stief, L. J.; Liebman, J. F.; Huie, R. E.; Kuo, S.-C.; Klemm, R. B. *J. Phys. Chem.* **1996**, *100*, 63.
(54) Herzberg, G. *Spectra of Diatomic Molecules*, 2nd ed.; Van Nostrand: New York, 1950.